High-Pressure Freezing Provides New Information on Human Epidermis: Simultaneous Protein Antigen and Lamellar Lipid Structure Preservation. Study on Human Epidermis by Cryoimmobilization

Stephan Pfeiffer, Gabriele Vielhaber, Jens-Peter Vietzke, Klaus-Peter Wittern, Ulrich Hintze, and Roger Wepf
Analytical Research Department, Beiersdorf AG Hamburg, Hamburg, Germany

Current transmission electron microscopy techniques do not permit simultaneous visualization of skin ultrastructure and stratum corneum extracellular lipids. We developed a new procedure, which entails application of high-pressure freezing followed by freeze-substitution with acetone containing uranyl acetate, followed by low temperature embedding in HM20. Electrospray ionization mass spectrometry showed that the amount of lipids lost during preparation was minimal. The ultrastructure of cryoprocessed skin was compared with that of conventionally prepared skin samples. Cryoprocessing, but not conventional processing, enabled visualization of lipid stacks within epidermal lamellar bodies, as well as the extracellular lipid domains of the stratum corneum and the ultrastructure within keratinocytes. Anti-filaggrin immunocytochemistry also showed, e.g., excellent preservation of filaggrin on cryoprocessed samples. Additionally, the cytosol of keratinocytes appeared to be organized in ''microdomain''-like areas. Finally, the stratum corneum appeared more compact with smaller intercellular spaces and hence tighter cell–cell interactions, after cryoprocessing, than after conventional tissue preparation for transmission electron microscopy. We conclude here that only cryoprocessing preserves skin in a close to native state. ***Key words: electron microscopy/filaggrin/high-pressure freezing/lamellar lipids.***
J Invest Dermatol 114:1030–1038, 2000

The stratum corneum (SC), often simplified according to a ''brick and mortar'' analogy, is essential for maintaining the permeability barrier of the skin (Elias, 1981; Wertz and Downing, 1982; Landmann, 1986). The protein filled corneocytes are embedded in an intercellular lipid-enriched matrix, composed mainly of ceramides, cholesterol, and fatty acids (Melnik *et al*, 1989; Lampe *et al*, 1983; Wertz and Downing, 1983). This unique barrier system regulates the transcutaneous water loss and the penetration of topically applied substances into the epidermis.

Breathnach (1973) first visualized the lipid-enriched structures in SC by freeze-fracturing for transmission electron microscopy (TEM). Elias and Friend (1975) showed that these lamellar lipids were localized to SC intercellular domains. This technique was further improved by Landmann *et al* (1981), Holman *et al* (1990), and Hofland *et al* (1995). Another important development for recording lipid bilayers was aldehyde fixation followed by OsO_4 postfixation, routine dehydration at room temperature, and Epoxy embedding (Elias and Friend, 1975; Fartasch, 1997; Menon and Ghadially, 1997). OsO_4 fixes the more polar lipids, e.g., the lamellar bodies (LB) in the stratum granulosum (SG) and the phospholipids in the cell membranes of keratinocytes; however, it fails to preserve or visualize the nonpolar lipids in the intercellular spaces of the SC. To visualize these lipids, RuO_4 postfixation was introduced (Madison *et al*, 1987; Hou *et al*, 1991; Van den Bergh *et al*, 1997). Because of its high reactivity, RuO_4 penetrates poorly into the SC, and tissue preservation can be unreliable (Schwartzendruber *et al*, 1995). Moreover, chemical fixation leads to distortion and reorganization of the native state of tissues (Plattner and Zingsheim, 1984; Robards and Sleytr, 1985). Chemical fixatives immobilize tissues over a period of seconds to minutes, during which detrimental chemical and osmotic changes can occur (Müller, 1992; Wilson *et al*, 1998). In addition, changes in cell and organelle membranes, and even extraction of lipids from membranes can occur (Weibull *et al*, 1983).

To overcome such changes in skin ultrastructure, and to minimize the loss of lipids during the different preparation steps, we applied cryopreparation involving high-pressure freezing, freeze-substitution, and embedding at low temperatures. With the high-pressure freezing technique, tissue samples of up to 200 μm thickness can be cryoimmobilized within 25–30 ms without the formation of detectable ice crystals (Studer *et al*, 1995; Hohenberg *et al*, 1996). In the following preparation procedure, however, fixatives must be used to prevent the loss of biologic material during the long-term low temperature dehydration and embedding steps (Schwarz *et al*, 1993; Walther *et al*, 1993).

The aim of this study was to develop a method of sample preparation, which allows both the visualization of all ultrastructural components by electron microscopy and the preservation of the antigenicity of skin samples.

Manuscript received October 11, 1999; revised February 10, 2000; accepted for publication February 16, 2000.

Reprint requests to: Dr. Stephan Pfeiffer, Analytical Research Department, Beiersdorf AG Hamburg, Unnastraβe 48, 20253 Hamburg, Germany.

Abbreviations: amu, atom mass unit; LB, lamellar bodies; SC, stratum corneum; SG, stratum granulosum; SP, stratum spinosum.

MATERIALS AND METHODS

To process native skin, biopsies (Ø 2 mm) were taken from the forearm of three different individuals ranging in age from 27 to 56 y. The tissue was stored in minimal essential medium (Gibco, Eggenstein, Germany) at 4°C during transport to the laboratory (Pfeiffer *et al*, 1996). The subcutaneous fat was removed and the epidermis subsequently cut with a razor blade into rectangular pieces of approximately $0.2 \times 0.5 \times 0.5$ mm. Care was taken to keep the tissue moist in minimal essential medium during handling.

Chemical fixation for routine TEM A quarter of each skin sample was prefixed overnight in modified Karnovsky's medium (Elias and Friend, 1975) at 4°C, washed twice with 0.2 M sodium cacodylate buffer for 10 min each, and postfixed with 1% (wt/vol) OsO_4 in 0.133 M sodium cacodylate buffer containing 0.5% (wt/vol) $K_4Fe(CN)_6$ at 4°C for 45 min. Where appropriate, 0.5% (wt/vol) RuO_4 was used instead of OsO_4. Subsequently, specimens were dehydrated in an ethanol series and embedded in Epon 812 (Luft, 1961). Polymerization was carried out overnight at 60°C.

High-pressure freezing and freeze-substitution for TEM The skin specimens were placed in the cavity (100 μm in depth) of a standard aluminum platelet filled with 1-hexadecene. The SC was aligned parallel to the bottom of the cavity and sandwiched with a second 100 μm platelet. The sandwich was inserted in the specimen holder and frozen in a high-pressure freezer (HPM 010 Bal-Tec, Balzers, FL; Moor and Hoechli, 1970; Müller and Moor, 1984). The frozen specimens were stored in liquid nitrogen until further processing. The subsequent freeze-substitution (at –90°C for 30 h, –70°C for 8 h, –50°C for 8 h) was performed using acetone as the substitution medium and uranyl acetate as the fixing agent in a conventional freeze-substitution unit (FSU 010 Bal-Tec, Balzers, FL). Before cooling down to –90°C, the substitution medium was saturated with uranyl acetate at room temperature. After removal of the frozen 1-hexadecene with a small precooled brush under liquid nitrogen, the specimens were transferred directly to transfer vessels (Hohenberg *et al*, 1994) and placed in 1.5 ml microfuge tubes (Eppendorf) filled with the substitution medium. After freeze-substitution the skin specimens were infiltrated with methacrylate (HM-20, Polysciences, Eppelheim, Germany) by the following protocol (at –50°C). Specimens were washed in pure acetone for 30 min before infiltration with 30% (vol/vol) HM-20/70% (vol/vol) acetone, and 70% HM-20/30% acetone for 2 h, followed by three incubations for 2 h each in pure HM-20. The ultraviolet-polymerization was carried out at –50°C for 48 h followed by a postpolymerization at room temperature for at least 3 d.

Ultramicrotomy at room temperature and TEM Thin sections were cut with a Reichert Jung Ultracut E microtome with a diamond knife (Diatome Switzerland), counterstained with uranyl acetate and lead citrate (Reynolds, 1963) and examined in a EM 912 Ω (Leo, Oberkochen, Germany).

Electrospray ionization mass spectrometry To determine the amount and composition of extracted material in the dehydration media, samples were analyzed by electrospray mass spectrometry (ESQUIRE, Bruker, Bremen, Germany) in a negative ionization mode. For this, the freeze-substitution media were diluted (1:2) with methanol containing 2 mM $NH_4(CH_3COO)$ and injected with a syringe pump into the mass spectrometer.

Lipid standard for mass spectrometry As the standard for human SC lipids a mixture of cholesterol, galactocerebroside, ceramide III, and oleic acid as described by Landmann (1985) was used. Five milligrams of ceramide III, 5 mg of galactocerebroside, 10 mg of oleic acid, and 10 mg of cholesterol were diluted in 500 μl of methanol/chloroform (1:2) and sonicated for 30 min. Subsequently, the solvent was removed by rotary evaporation for 1 h at 40°C, then 10 ml of 0.1 M Tris–HCl (pH 8.1) were added to the lipid film. The resulting two-phase system was sonicated five times for 10 min at room temperature, giving an oil in water emulsion with a final lipid concentration of 3 mg lipid per ml.

Immunofluorescence and immunogold labeling All steps were performed at room temperature and all dilutions were prepared in washing buffer. Controls were performed by the application of bovine serum albumin instead of the primary antibody. A monoclonal antibody recognizing both profilaggrin and filaggrin was used (Harbor Bio-Products, Norwood, MA).

Immunofluorescence Two hundred nanometer sections were prepared, placed on glass coverslips and treated with 1% (wt/vol) bovine serum albumin in washing buffer [0.1% (vol/vol) Tween 20 in phosphate-buffered saline] for 60 min in order to prevent nonspecific binding. The primary antibody (diluted 1:50) was then applied for another 60 min. After washing four times with washing buffer the sections were incubated with a Cy3-conjugated sheep-anti-mouse IgG secondary antibody (Dianova, Hamburg, Germany) (diluted 1:1000) for 60 min. The samples were washed again and stained with 4′,6-diamindino-2-phenylindol (50 μg per ml phosphate-buffered saline) for 15 min for visualization of nuclei. After washing three times the samples were fixed on slides with MOWIOL and analyzed with a Zeiss Axioskop 35 fluorescence microscope.

Immunogold labeling The ultrathin sections were placed on copper grids and processed in a grid-box as described above for the immunofluorescence studies except that the number of the washing steps was doubled. Blocking was performed with 3% (vol/vol) normal goat serum (DAKO, Hamburg, Germany). The primary antibody was diluted 1:25 and the secondary antibody (10 nm gold-conjugated goat-anti-mouse IgG) (DAKO) 1:100. Finally, the sections were poststained with uranyl acetate and lead citrate and investigated with a EM 912 Ω (Leo).

Measurement of the lipid lamellae distance The lamellar distances of the lipid lamellae in the ultrathin sections were measured directly on digital micrographs with the "NIH-Image" software version 1.60, National Institutes of Health.

RESULTS

SC The surface contours of chemically fixed corneocytes (**Fig 1*a***) show an undulated surface (arrow in **Fig 1*a***), and hence a wide intercellular space between adjacent corneocyte layers (asterisk in **Fig 1*a***). In contrast, the SC of cryoimmobilized samples (**Fig 1*b***) exposes less undulated and smoother cell contours. As a consequence, the intercellular spaces are remarkably reduced, and fine structures on the surface, such as cavities (*white arrow*) come into focus. In addition, as a consequence of this compact packing, the interdigitated cell envelopes of adjoining corneocytes in one and the same corneocyte layer (*black and white arrow* in **Fig 1*b***) are resolved much easier in cryoimmobilized samples. Intercellular electron-dense corneosomes (*black arrow*) can be found throughout all of the corneocyte layers in the SC of cryoimmobilized samples. In contrast, in chemically fixed samples, these opaque structures were concentrated only in preserved adjacent layers of the SC, due to the artifactual separation of corneocytes. Moreover, in cryoimmobilized samples, keratin can be seen as fine arrays of filaments even in the outermost SC. Interestingly, in the bottom layers (1–3) of freeze-substituted SC, corneocytes are less transparent, whereas in the upper layers the transparency increases, as shown throughout **Fig 1(*b*)**. In chemically fixed samples, the image contrast increases inversely: the lower part of the SC is electron transparent whereas towards the skin surface the corneocytes become more electron-dense.

Stratum spinosum (SP) Ribosomes and filament aggregates are homogeneously distributed throughout the cytoplasm after chemical fixation of the tissue (**Fig 2*a***). Filament aggregates appear as very compact structures (arrow) and therefore individual filaments are hardly resolvable. In contrast, in cryoimmobilized samples, the keratin filaments are organized in dense or loose bundles in such a way that individual filaments can be still resolved (arrow in **Fig 2*b***). In addition, ribosomes are organized into "domain-like clusters" embedded in a structurally highly organized cytoplasm (asterisk in **Fig 2*b***). Organelle membranes, however, are less prominent, barely stained and appear neither undulated nor irregular in cryoimmobilized samples. In contrast, in conventionally fixed samples, membranes are often undulated and clearly separated from the cytoplasm, e.g., the outer membranes of mitochondria and their christae. Finally, in the core of nuclear pores, conical areas of less density appear to protrude from the nucleoplasm into the cytoplasm only in cryoimmobilized samples.

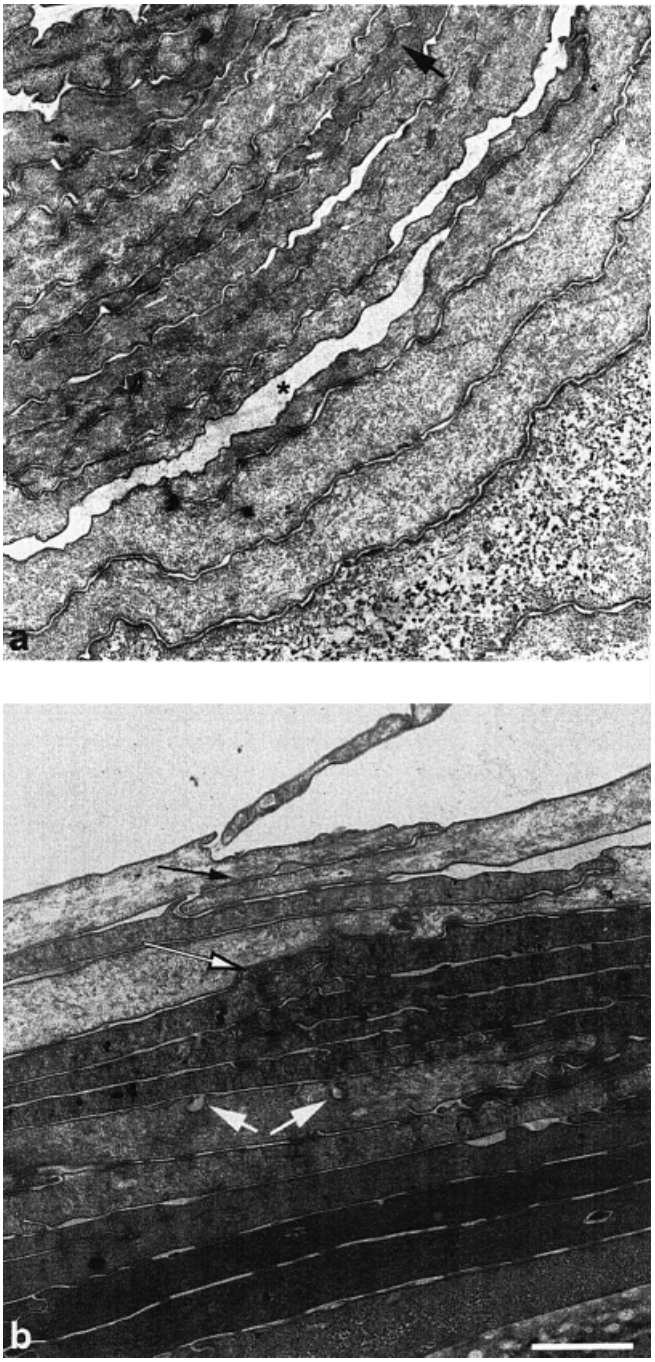

Figure 1. The SC ultrastructure after chemical fixation and dehydration at room temperature *versus* the ultrastructure after cryoprocessing. (*a*) SC after chemical fixation and dehydration at room temperature. The surface contour shows a more undulated surface (*arrow*) and hence a wider intercellular space between the corneocytes (*asterisk*) compared with cryoimmobilized and freeze-substituted skin (*b*). The surface contours are smoother, the intercellular space is reduced, and some cavities (*white arrows*) on the surface of the corneocytes become visible. The intercalated membrane structures of adjoining corneocytes in one and the same layers (*black/white arrow*) and intact corneodesmosomes (*black arrow*) throughout all layers in the SC (*scale bar*: 2 μm) are preserved.

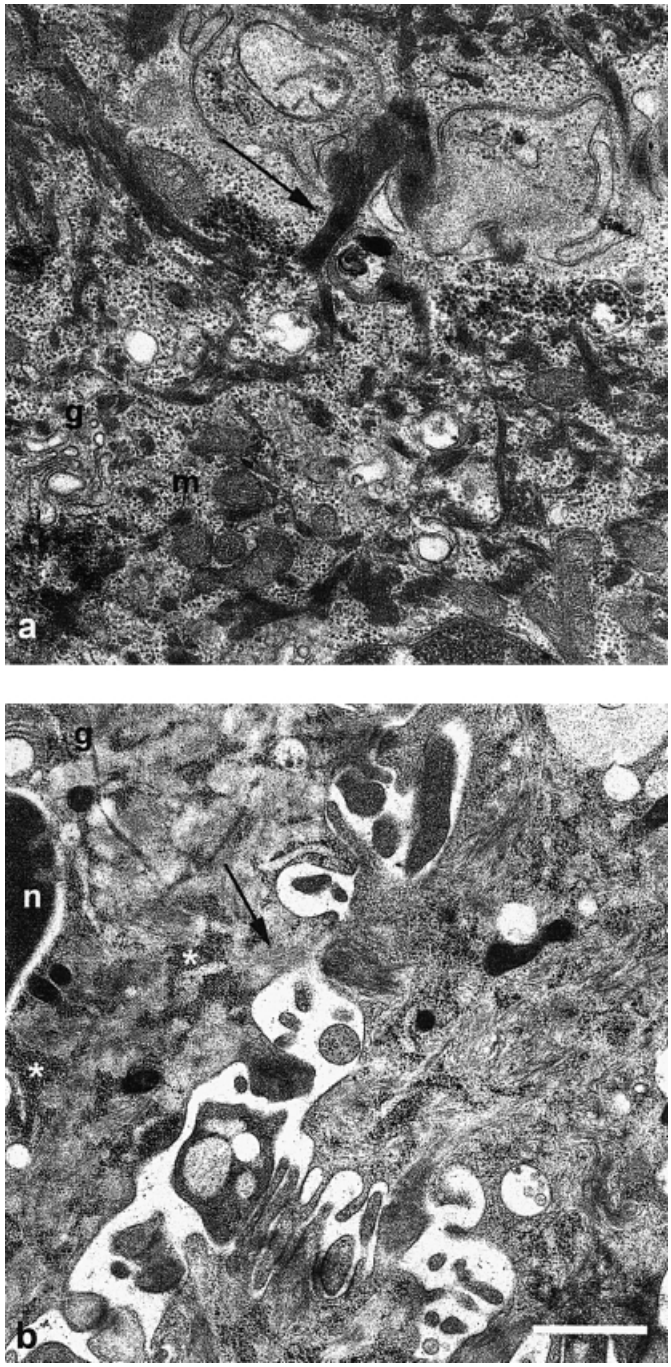

Figure 2. The SP ultrastructure after chemical fixation and dehydration at room temperature *versus* the ultrastructure after cryoprocessing. In chemically fixed keratinocytes in the SP (*a*), the ribosomes are homogeneously distributed over the whole cytosol, and keratin filaments are visible as bundled compact structures (*arrow*). Single filaments are hardly distinguishable. In contrast, in cryoprocessed samples (*b*) single keratin filament structures (*arrow*) are clearly resolved. The cytoplasm is organized in distinct clusters (*asterisk*), e.g., ribosome free areas *versus* clusters of ribosomes (m, mitochondria; n, nucleus; g, Golgi complex; *scale bar*: 0.75 μm).

Cellular organization in cryoprepared epidermis A dense arrangement of structures, e.g., filaments, ribosomes, and vesicles in distinct clusters or ''microdomains'', is found throughout the nucleated layers of the epidermis, from the basal layer up to the interface between the SG and the SC (**Fig 3*a***).

In a basal-apical direction, the intercalating space of plasma membranes between adjacent keratinocyte layers are reduced throughout the epidermis (e.g., *white arrow*s in **Fig 3*a***.). As cell protrusions become less extended, less voluminous intercellular space exists between intercalating keratinocytes. The intercellular spaces reach a minimum in between the upper SC layers. **Figure 3(*b*)** depicts the cytosol of a corneocyte in the outermost layer of the SG. Fine filament structures (f) and ribosomes in distinct areas are visible even at this late stage of differentiation. The asterisk indicates an area where the microfilament organization in

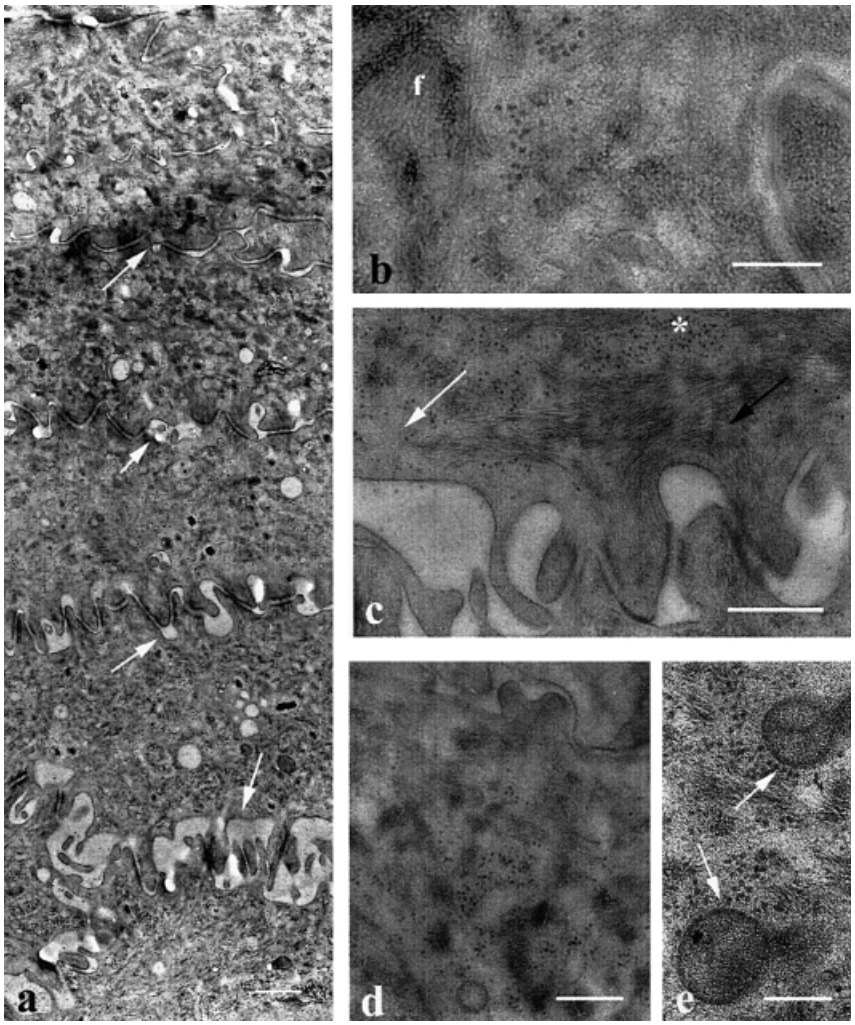

Figure 3. Cytoplasma organization after high-pressure freezing, freeze-substitution, and embedding in HM20. The intracellular organization into ''microdomain structure'' is visible throughout all layers of the SP. The undulated membranes of keratinocyte cell protrusions become smoother towards the skin surface. As a consequence the intercalations of plasma membranes between lateral adjacent keratinocyte layers are reduced vertically (*white arrows*) as well as laterally (*scale bar*: 0.75 μm). (*b*) Fine filament structures (f) in the cytoplasm of a corneocyte in the outermost layer of the SG are found (*scale bar*: 250 nm). (*c*) Depicts a keratinocyte from a central layer of the SP in which ribosome-free areas (*white arrow*) and clusters of ribosomes (*), are found (*scale bar*: 200 nm) in the cytosol. Beneath desmosomal plaques single filament structures (*black arrow*) are arranged parallel to the direction of the protruding plasma membrane. (*d*) Also in the lower layers of the SP ribosomes, filaments and ribosome free areas could be distinctly located (*scale bar*: 200 nm). (*e*) Mitochondria show less christae structures (*white arrows*, *scale bar*: 250 nm).

the cytoplasm is obscured artifactually by a segregation pattern due to ice crystal formation in this area. We did not find any keratohyalin granules in cryoprocessed epidermis (**Figs 7*a***, **3*b***). **Figure 3**(***c***) depicts a keratinocyte within the mid-layer of the SP in which the cytosol shows ribosome-free areas (*white arrow* in **Fig 3*c***), as well as clusters of ribosomes (asterisk). Beneath desmosomal plaques, single filaments (*black arrow* in **Fig 3*c***) are arranged parallel to the direction of the protruding plasma membrane.

SC/SG interface and SC extracellular domains after conventional preparation The keratin filaments in the uppermost SG layer appear as electron-dense bundles (arrow in **Fig 4*a***) either loose in the cytosol or connected to desmosomal remnants. Such corneodesmosomes are visible between the lowermost corneocytes and the outer SG cell, but show very few structural details (*bold arrow* in **Fig 4*a***). In addition, the key steps of extracellular lamellar bilayer formation, the fusion of LB with an apical plasma membrane of an outer SG cell can be observed (**Fig 4*a***, ***b***). The lamellar stacks in the LB appear as a series of electron-dense and -lucent lines with an interlamellar spacing of 3.81 ± 0.71 nm. As lamellar structures cannot be detected in the intercellular spaces of the SC in conventionally preserved samples poststained with OsO_4, RuO_4 postfixation was used (**Fig 4*d***, ***e***). This allowed visualization of the characteristic alternating, electron-dense and electron-lucent lamellar structures (**Fig 4*d***, ***e***) in the SC intercellular spaces. The spacing between the electron-dense lines is 5.14 ± 0.60 nm. Other morphologic features are largely destroyed by RuO_4 treatment. In such samples, the cytosol of corneocytes, show two different regions of ultrastructural preservation (*black and white arrow* in **Fig 4*c***).

SC/SG interface and SC extracellular domains after cryopreparation Samples were prepared using the method with a minimal extraction potential (see below) and without the use of oxidative fixatives such as RuO_4 or OsO_4. As shown in **Fig 5**(***a***), LB in the SP as well as in the extracellular domains between corneocytes are visible after high-pressure freezing, freeze-substitution, and embedding at low temperatures in methacrylate (HM20). This method makes it possible to visualize simultaneously the lamellas in the LB of the SP as clearly as the filament bundles of the intermediate filaments and other cellular components in the same cell.

At the interface between the SG/SC (**Fig 5*a***), desmosomes, extruded LB content and intercellular lamellar domains are revealed. The membrane structures of desmosomes, the bilayers of the cell membranes (arrows in **Fig 5*a***), a central mass line, and

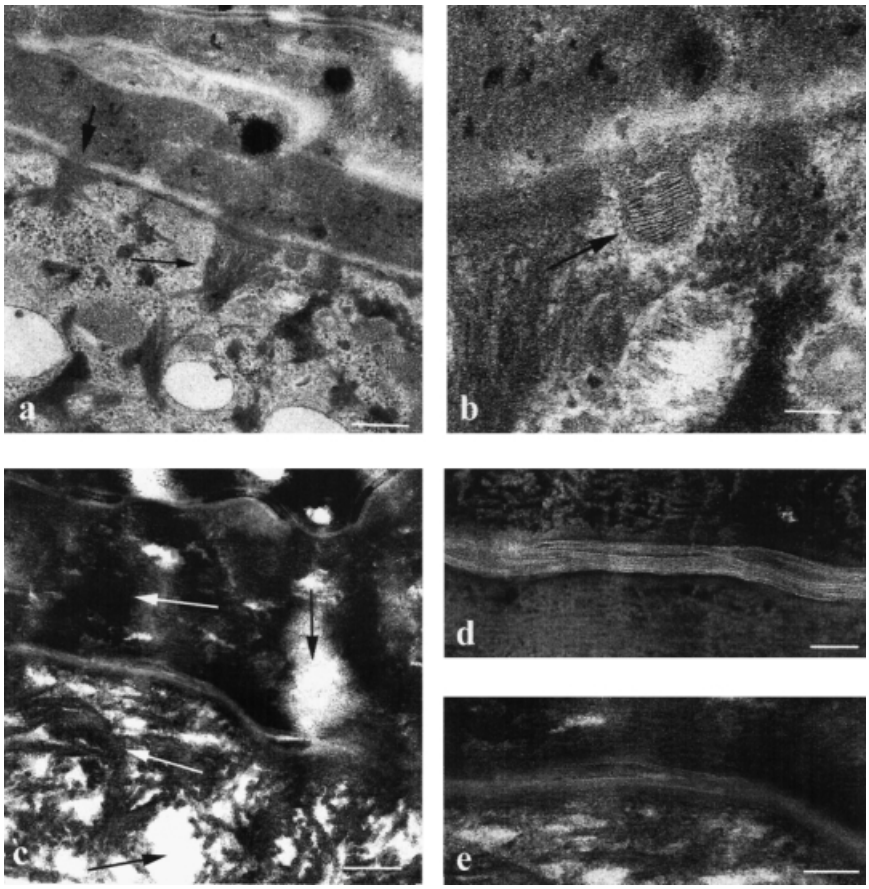

Figure 4. Interface between SG/SC after chemical fixation and dehydration at room temperature and embedding in Epon. (*a*) The cellular organization at the level where the LB are extruded is shown after postfixation with OsO_4. Keratin filaments appear as electron-dense bundles (*arrow*) and are found loosely in the cytoplasm or connected to desmosomal remnants. Corneodesmosomes expose very little structural details (*bold arrow*). (*b*) A LB (*a*) fused with the plasma membrane (*scale bar*: 400 nm). The lamellar stacks in the LB have a spacing between the electron-dense lines of 3.81 ± 0.71 nm (*scale bar*: 150 nm). (*c–e*) The ultrastructure of the intracellular lipid lamellae becomes only visible after postfixation with RuO_4. In such samples, the cytoplasm of corneocytes shows two different regions of ultrastructural preservation, electron-dense areas of ''compressed'' filament structures (*white arrow*) and electron-lucent areas in which any biologic material appears to be absent (*black arrow*) (*scale bar*: 250 nm). The extracellular lipid arrangements (*d*, *e*) are visible as characteristic alternating electron-dense and electron-lucent structures. The distances between the electron-dense lines is 5.14 ± 0.60 nm (*scale bar*: 220 nm).

the connection to the intermediate filaments as described by Schmidt *et al* (1994), are all clearly recognizable. Some LB show the characteristic electron-dense and -lucent lines, known as lipid stacks, over the whole volume, whereas others show regular structures only within a part of their lumen. In general, the limiting membrane of the vesicle clearly separates the LB contents from the cytosol (**Fig 5*b***). We have measured a regular spacing between the electron-dense lines of 4.99 ± 0.94 nm in the LB. The vesicular membrane has a spacing of 4.88 ± 0.76 nm. **Figure 5*c*** depicts an LB in the process of extruding its lamellar content into the intercellular space. In **Fig 5*d*** the lamellar stacks of extruded LB can be observed between the lamellar lipid layers in the intercellular space, depicting an intermediate state before the lipids of the LB are rearranged into the lamellar bilayer stacks. The lipid domain in the intracellular space in the SC can be visualized as characteristic alternating electron-dense and electron-lucent structures with a spacing between the electron-dense lines of 5.34 ± 1.15 nm.

Lipid preservation by cryoprocessing Preliminary attempts to visualize the LB lamellar and intercellular lamellar membranes in the SC of cryoprocessed skin samples failed (not shown), presumably due lipids loss during low temperature dehydration and embedding steps. To investigate the loss of lipids, the extent of lipid extraction during freeze-substitution was analyzed by mass spectroscopy (electrospray ionization mass spectrometry, neg. mode) of the remaining substitution media. The extracted molecules found in the substitution media of human skin samples have a mass of 170–750 amu. A mixture of human SC skin lipids (Landmann, 1985), containing free fatty acids, ceramides, and cholesterol was utilized as a standard (**Fig 6*d***). The mass spectra of the lipid mixture shows significant peaks at 311, 325, 339, etc., representing eicosanoic acid C20:0 (311), heneicosanoic acid C21:0 (325), docosanoic acid C22:0 (339). As the mass of 311 (**Fig 6*a***, ***b***), corresponds to a free fatty acid, and the difference between significant peaks is 14 amu, corresponding to a CH_2 group, these spectra represent most likely the extracted lipids in the freeze-substitution media. **Figure 6(*b*)** shows that the total lipid loss is significantly reduced, if the final substitution temperature was kept at –90°C rather than 20°C. A further reduction of the total amount of extracted lipids, as well as a change in the mass pattern, was found when uranyl acetate was added to the freeze-substitution medium (**Fig 6*c***). These observations demonstrate that the amounts of extracted lipids clearly depends on the final temperature reached during freeze-substitution, as well as on the use of uranyl ions as fixatives during the dehydration step.

Immunocytochemistry To investigate the preservation of antigenicity, an antibody against profilaggrin and filaggrin and a secondary antibody linked with Cy3 for immunofluorescence microscopy or alternatively with 10 nm gold for electron microscopy was used. Double staining with 4′,6-diamindino-2-phenylindol makes it possible to distinguish between the nucleated cell layers of the vial epidermis and the SC. The fluorescence labeling reflects the known expression of (pro-)filaggrin (**Fig 7*d***). The granular staining extends from the uppermost two layers of the SG up to the lower six to seven layers of the SC. Concomitantly,

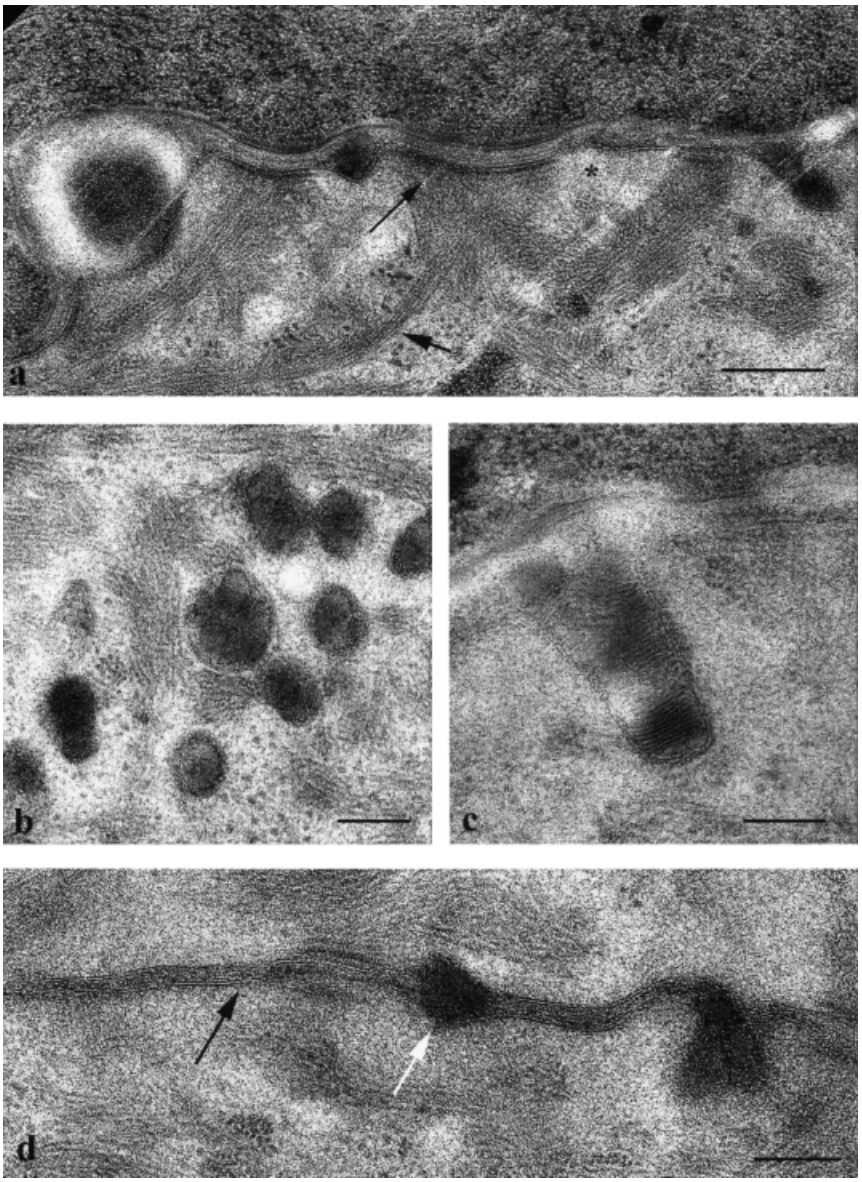

Figure 5. Interface between SG/SC after high-pressure freezing, freeze-substitution, and embedding in HM20. (*a*) The membrane structures within desmosomes, the lipid bilayers of the cell membrane, and the anchoring plaques between the intermediate filaments and the desmosomes are clearly resolved. The lipid bilayer is associated with a dense plaque (*arrow*) to which single keratin filaments are linked. In the cytoplasm ribosome free areas (*asterisk*), distinct clusters of ribosomes and filament structures (*bold arrow*) are found (*scale bar*: 400 nm). (*b*) Different structural details in the contents of intracellular LB can be seen. Some LB show the characteristic electron-dense and electron-lucent lines of lipid stacks over the whole volume, whereas others show these regular structures only in a part of their lumen. The regular spacing between the electron-dense lines is 4.99 ± 0.94 nm. The bilayer of the vesicles has a spacing of 4.88 ± 0.76 nm (*scale bar*: 100 nm). (*c*) LB in the process of extruding its lamellar contents into the intercellular space. Here the lamellar structures can be resolved until they are extruded into the intercellular space, which itself shows no lamellar arrangement (*scale bar*: 80 nm). (*d*) Some lamellar stacks of extruded LB can be observed between the lamellar lipid layers in the intercellular space. The lipid domain in the intracellular space in an outer SC layer can be visualized as the characteristic alternating electron-dense and electron-lucent structure with a spacing between the electron-dense lines of 5.34 ± 1.15 nm (*scale bar*: 150 nm).

staining intensity increases up to an extremely strong labeling of the fifth and sixth layer of the SC. With the transition to the next SC layer the staining decreases sharply.

By immuno-EM, the same labeling distribution, with a gradual increase in label density was observed (**Fig 7*a***), as with immunofluorescence microscopy. No significant labeling was observed in control sections incubated with bovine serum albumin instead of the primary antibody. In general, in comparison with unlabeled skin samples (**Fig 2**), the fine structural details appear blurred after immunogold labeling and their contrast is reduced. Statistical analysis of the number of gold particles in the labeled layers revealed that the staining intensity increased by up to 30% from the first labeled granular layer to the most intensively stained cornified layer. Whereas labeling was clearly associated with intracellular filamentous structures in the SC, there was no apparent correlation with cellular structures in the SG; however, no remarkable clustering of the gold particles on structural components, such as the granular staining pattern of keratohyalin suggested in light microscopical images, was found.

DISCUSSION

Morphologic preservation We have shown that high-pressure freezing followed by freeze-substitution and embedding at low temperatures can yield human epidermis samples with excellent structure preservation. Intracellular fine structure as well as lamellar lipid structures in the SC intracellular space can be visualized simultaneously with just one preparation technique.

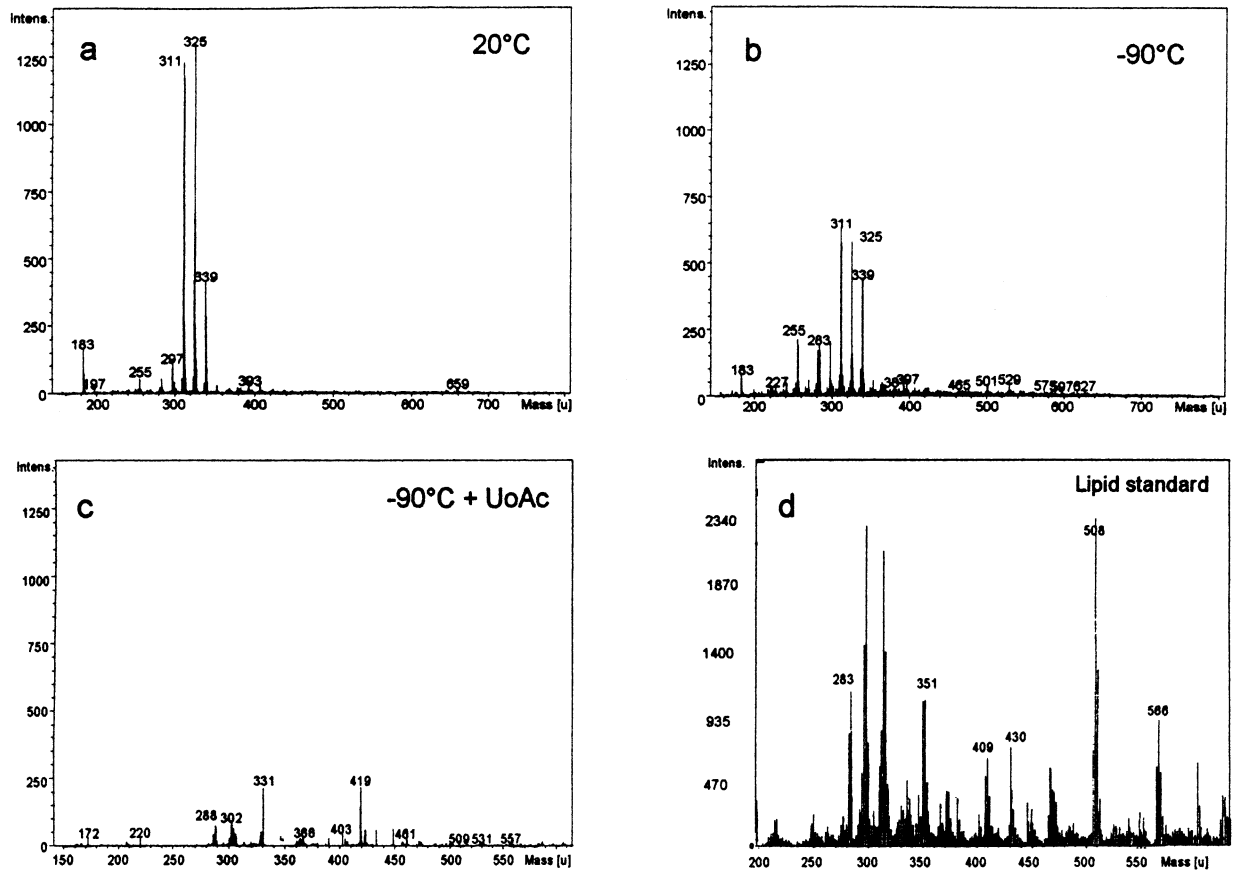

Figure 6. Mass spectrometry. (*a*) Shows the total mass between 150 and 700 amu for a final substitution temperature of 20°C. The total mass is significantly reduced if the dehydration temperature is reduced to –90°C as in (*b*). A further reduction of the total amount of extracted lipids as well as a change in the mass pattern was found when uranyl acetate was added to the freeze-substitution medium (*c*). A mixture of human SC skin lipids, containing free fatty acids, ceramides, and cholesterol was investigated as the standard (*d*). The mass spectra of the lipid mixture shows significant peaks at 311, 325, 339, etc., representing eicosanoic acid C20:0 (311), heneicosanoic acid C21:0 (325), docosanoic acid C22:0 (339).

In contrast, chemical fixation at room temperature induces extensive artifacts on various cellular structures. During fixation, a concentration gradient of fixative is built up which leads to a gradual fixation, starting at the cell surface and ending towards the center of the nucleus. This gradual process changes the ion concentration, the osmolarity and the pH in each cell before it is completely chemically cross-linked. As a consequence, reorganization of cellular components and the cytoplasm occurs, e.g., the displacement of ribosomes or filament bundles (**Fig 2**). Finally, three-dimensional cross-linking with glutaraldehyde may also cause a condensation of cellular components resulting in shrinkage of the cells and a subsequent disruption of intercellular structures such as the corneosomes (**Fig 1*a***). Complete dehydration at room temperature is an additional source of shrinkage artefacts for tissues (Cohen, 1979; Kellenberger, 1987). Such large volume changes leads to deformation of the corneocytes and the SC (**Fig 1*b***) and to an aggregation of filament structures. From control experiments of chemically fixed skin, which were not dehydrated at room temperature but high-pressure frozen and freeze-substituted, we know that the major delocalization of cellular components and shrinkage of organelle membranes already appears after chemical fixation and not after dehydration at room temperature (results not shown). Therefore, we can conclude that the major reorganization of cell components take place during the chemical cross-linking process, whereas the large-scale changes take place during dehydration at room temperature.

OsO_4 and RuO_4 are frequently used to visualize the lipid sheets in the LB and intercellular lipid structures in the SC of conventionally prepared skin samples (Elias, 1981; Landmann, 1985). OsO_4 reacts preferentially with the C=C bonds in unsaturated hydrocarbon chains and with the sugar moieties of glycoceramides (Altman, 1894; Plattner and Zingsheim, 1984). Hence, OsO_4 fixes the lipid sheets in the LB and the single lipid discs in the intercellular space; however, it fails to fix the intercellular lamellar domains. As the degree of unsaturation of the lipid hydrocarbon chains does not change during transformation of the lipid discs into the intercellular lamellae (Lampe *et al*, 1983), this observation reflects the accompanying enzymatic transformation of glucosylceramides into ceramides.

It is well known that the penetration of RuO_4 into the SC is very poor (Schwartzendruber *et al*, 1995). The high reactivity of RuO_4 with all organic material, especially the strong oxidation of proteins, results in a condensation of protein structures and hence a build up of an additional diffusion barrier for RuO_4. To optimize the visualization of these lipid structures in the SC, different protocols for room temperature preparation have been invented (Van der Meulen *et al*, 1996; Wijdeveled *et al*, 1996; Fartasch, 1997; Van den Bergh *et al*, 1997) allowing comparable structure preservation. The main disadvantage of staining and fixing with RuO_4 remains, however, which is the reduction of the ultrastructural information by a heavy staining and condensation of nonlipid areas (**Fig 4*c***). RuO_4 staining therefore only improves the visualization of the lipid multilayer structures in the SC.

The loss of lipids during dehydration can be reduced considerably by decreasing the final temperature of the freeze-substitution process (**Fig 5**), and by the simultaneous use of fixatives (Humbel and Müller, 1984). With the use of uranyl acetate as a fixing and staining agent during dehydration at low temperatures, the lamellar sheets in the LB as well as the intercellular lamellar domains can be visualized. The differences between the spacings of the membrane stacks in LB and in the intercellular lamellar domains after cryopreparation and conventional processing may be due to

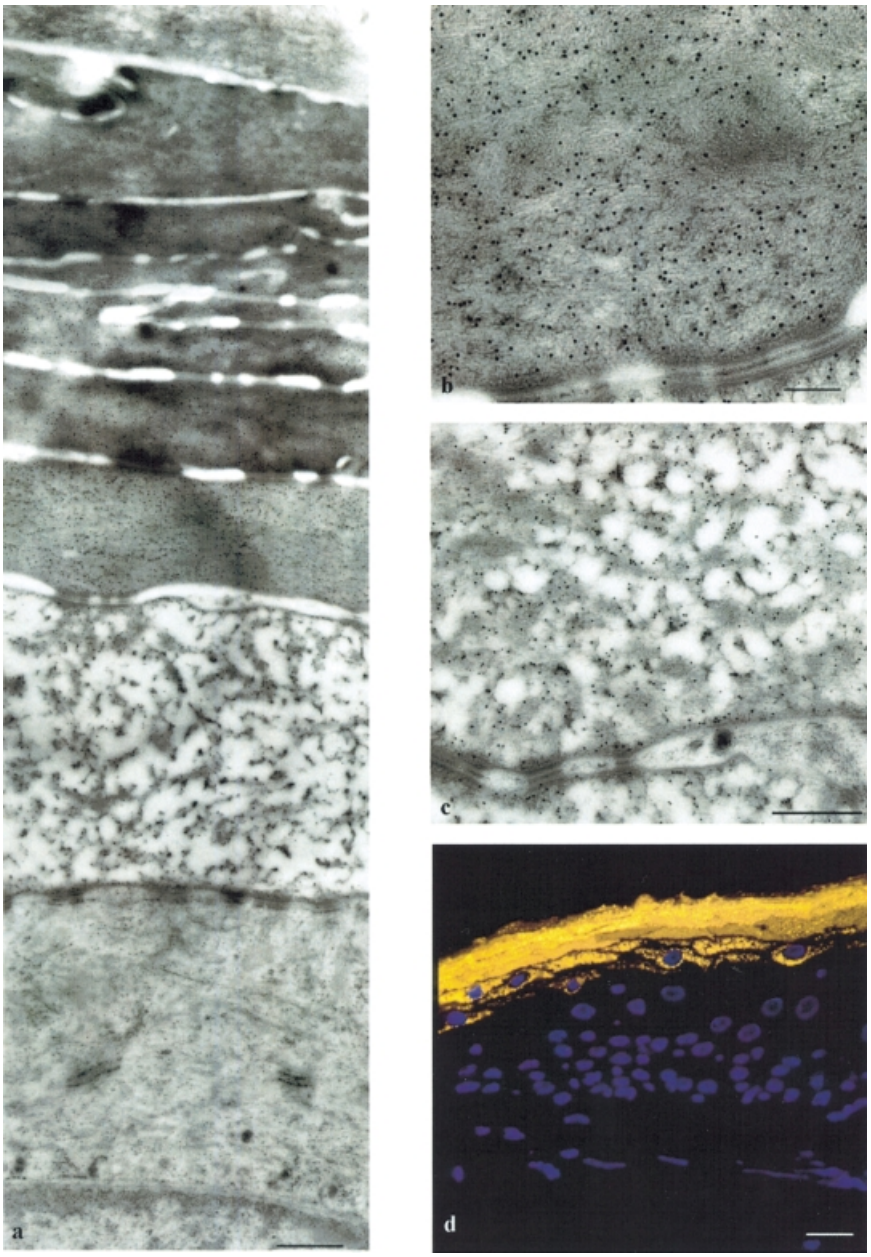

Figure 7. Immunofluorescence and immunoelectron microscopy for filaggrin in cryoprocessed skin. The labeling of filaggrin in immunofluorescence microscopy shows the known distribution of filaggrin in the uppermost two layers of the SG up to the sixth to seventh lower layers of the SC, with the staining intensity increasing accordingly. Staining of the nuclei with 4′,6-diamindino-2-phenylindol (*blue*) makes it possible to distinguish between the viable epidermis and the SC (*d*) (*scale bar*: 25 μm). In immuno-TEM (*a*), the same labeling distribution and gradual increase in concentration was found (*scale bar*: 1000 nm). Whereas the labeling in the SC was clearly associated with intracellular filamentous structures (*scale bars*: (b) 200 nm; (*c*) 500 nm), there was no apparent correlation with any cellular structure in the SG. n, nucleus.

the different dehydration procedures or cross-linking procedure and has to be further investigated. To reduce further the extraction of lipids during embedding of the skin tissue we used HM-20 and ultraviolet light polymerization at −50°C according to Weibull *et al* (1983), who has demonstrated a significant reduction of lipid extraction using this resin.

Another striking difference between conventional and cryo-preparation is the change in contrast of the stained membranes. In conventionally prepared samples, membranes of cell organelles are visible as one or two dark lines separated by a lucent line in the middle, e.g., plasma membrane or the mitochondria membranes (**Fig 3*e***); furthermore, the membrane contours are highly undulated (**Fig 2*a***). In cryoprocessed samples the membranes generally show straighter contours and are visible as lucent lines surrounded by a dark stained cytosol. In our high-pressure frozen samples we occasionally found well preserved cell layers and such with segregation patterns in direct vicinity. These results can be explained by the different concentrations of glucose in the cells at the SC/SG interface (Gerhardi, 1983) and the high protein and low water concentration (< 10%) in the upper layers of the SC (Warner *et al*, 1988).

The phenomena of cytoplasmic organelles organized into ''microdomains, which is found throughout cryoprocessed epidermis from the basal layer up to the SC, indicates a new feature of structural organization of the cytoplasm. In such samples, the ''live–death'' transition zone is characterized by a highly organized cytoplasm with intact cell organelles at the last cell layer of the SG, followed directly by the first cornified cell layer of the SC. This indicates a high level of metabolism up to the last layer of the SG and a sharp localized transformation into cornified keratinocytes within only one cell layer.

Immunocytochemistry Immunocytochemical investigations confirm the high capability of cryoprocessing for good structure preservation. We found the same general expression pattern of (pro-)filaggrin as previously described (Günzel *et al*, 1991) for chemically fixed skin dehydrated at room temperature and embedded in LR-White: e.g., an increase of filaggrin from the SG to the sixth to seventh layer of the SC. In contrast to Günzel and coworkers, however, we did not find an aggregation of (pro-) filaggrin staining into keratohyalin granules in the SG, which are characteristic structures in chemically fixed samples. The fact that they are found after chemical fixation and subsequent cryoprocessing (data not shown) indicates that the existence of keratohyalin granules of which the main constituent is profilaggrin has to be considered as an artifact induced by chemical fixation. Previous work has already shown that there is no functional relationship between profilaggrin/filaggrin expression and keratin clumping (Weidenthaler *et al*, 1993; Ishida-Yamamoto *et al*, 1994).

In summary, we have demonstrated that only cryoprocessing makes it possible to preserve the ultrastructure close to the native state and enable the visualization of both intracellular and intercellular lipid domains with one and the same preparation technique. It is now possible to investigate ultrastructural components of skin at the electron microscopic level as well as to perform immunocytochemistry, for light and electron microscopy, with the same specimen. The new findings of ''microdomains'' in the cytoplasm of skin and the biologic function of filaggrin needs to be further investigated in order to elucidate their functional background.

We thank H. Hohenberg for excellent support in the high-pressure freezing technique and for discussion on compact tissue organization. Human skin was kindly provided by F. Pflücker, Department of Dermatology, Photodermatology Group, University Hospital Eppendorf, Hamburg. Furthermore we thank Prof. P. Elias and Prof. A. Kligman for critically reading the manuscript. This work was supported by the BMBF grant 13N66921.

REFERENCES

Altman R: *Die Elementarorganismen und ihre Beziehungen zu den Zellen*. 2te Auflage Veit, Leipzig, 1894, pp 76–96

Boyde A, Maconnachie E: Morphological correlation with dimensional change during SEM specimen preparation. *Scanning Electron Microsc* IV:27–34, 1981

Breathnach AS: Application of the freeze-fracture replication technique to investigative dermatology. *Br J Dermatol* 88:563–574, 1973

Cohen AL: Critical point drying—principles and procedures. *Scanning Electron Microsc* II:303–324, 1979

Elias PM: Epidermal lipids, membranes and keratinization. *J Dermatol* 20:1–19, 1981

Elias PM, Friends DS: The permeability barrier in mammalian epidermis. *J Cell Biol* 65:185–189, 1975

Fartasch M: Ultrastructural of epidermal barrier after irritation. *Microsc Res Techn* 37:193–199, 1997

Gerhardi S: *Die Charakterisierung von Kohlenhydraten in der menschlichen Hornschicht mittels Lectinen*. FH Hamburg-Bergedorf: Diplomarbeit, 1983, pp 23–29

Günzel S, Weidenthaler B, Hauβer I, Anton-Lamprecht I: Keratohyalin granules are heterogeneous in ridged and non-ridged human skin: evidence from anti-filaggrin immunogold labelling of normal skin and skin of autosomal dominant ichthyosis vulgaris patients. *Arch Dermatol Res* 283:421–432, 1991

Hofland HEJ, Bouwstra JA, Boddé HE, Spies F, Junginger HE: Interactions between liposomes and human stratum corneum in vitro: freeze-fracture electron microscopical visualization and small angle X-ray scattering studies. *Br J Dermatol* 132:853–856, 1995

Hohenberg H, Mannweiler K, Müller M: High-pressure freezing of cell suspensions in cellulose capillary tubes. *J Microsc* 175(I):34–43, 1994

Hohenberg H, Tobler M, Müller M: High-pressure freezing of tissue obtained by fine-needle biopsie. *J Microsc* 183(I):133–139, 1996

Holman PB, Spies F, Boddé HE: An optimized freeze-fracture replication procedure for human skin. *J Invest Dermatol* 94:332–335, 1990

Hou SYE, Mitra AK, White SH, Menon GK, Ghadiallay R, Elias PM: Membrane structures in normal and essential fatty acid-deficient stratum corneum: characterization by ruthenium tetroxide staining and X-ray diffraction. *J Invest Dermatol* 96:215–223, 1991

Humbel BM, Müller M. Freeze substitution and low temperature embedding. In: Müller M, Becker PR, Boyde A, Wolosewick JJ (eds). *The Science of Biological Specimen Preparation*. Scanning Electron Microscopy Inc., AFM O'Hara, 1984, pp 175–183

Ishida-Yamamoto A, Eady RAJ, Underwood RA, Cale BA, Holbrook KA: Filaggrin expression in epidermolytic ichthyosis (epidermolytic hyperkeratosis). *Br J Dermatol* 131:767–779, 1994

Kellenberger E. The response of biological macromolecules and supramolecular structures to the physics of specimen cryopreparation. In: Steinbrecht RA, Zierold K (eds). *Cryotechniques in Biological Electron Microscopy*. 1987, pp 35–87

Lampe MA, Williams ML, Elias PM: Human epidermal lipids: characterization and modulations during differentiation. *J Lipid Res* 24:131–140, 1983

Landmann L: Epidermal permeability barrier: transformation of lamellar granule-disks into intercellular sheets by a membrane-fusion process, a freeze-fracture study. *J Invest Dermatol* 87:202–209, 1986

Landmann L: Permeabilitätsbarriere der Epidermis. Grosse Scripta. In: Schirren C, Kreysel H-W (eds). Berlin: Grosse-Verlag, 1985, pp 116–126

Landmann L, Stolinski C, Martin B: The permeability barrier in the epidermis of the grass snake during resting stage of the sloughing cycle. *Cell Tissue Res* 215:369–382, 1981

Luft JH: Improvements in epoxy resin embedding methods. *J Biophys Biochem Cytol* 409–414, 1961

Madison KC, Schwartzendruber DC, Wertz PW, Downing DT: Presence of intact intercellular lipid lamellae in the upper layers of the stratum corneum. *J Invest Dermatol* 88:714–718, 1987

Melnik BC, Hollmann J, Verhoeven B, Plewig G: Microanalytical screening of all major stratum corneum lipids by sequential high-performance thin-layer chromatography. *J Invest Dermatol* 92(2):231–234, 1989

Menon G, Ghadially R: Morphology of lipid alterations in the epidermis: a review. *Microsc Res Techn* 37:180–192, 1997

Moor H, Hoechli M. The influence of high-pressure freezing on living cells. In: Favard P (ed.) *Proceedings of the 7th International Congress of Electron Microscopy Grenoble*. Paris: Société Francaise de Microscopie Électronique, 1970, 1: pp 445–446

Müller M: The integrating power of cryofixation-based electron microscopy in biology. *Acta Micrscópica* 1:37–44, 1992

Müller M, Moor H. Cryofixation of thick specimens by high-pressure freezing. In: Revel JP, Barnad T, Haggis GH (eds). *The Science of Biological Specimen Preparation for Microscopy and Microanalysis*. Scanning Electron Microscopy Inc., AFM O'Hara, 1984, pp 131–138

Pfeiffer S, Pflücker F, Hölzle E: Influence of pre-fixation storage conditions on the ultrastructure of pig skin and on the surface of human corneocytes. *Arch Dermatol Res* 288(5–6):312, 1996

Plattner H, Zingsheim HP: *Elektronenmikroskopische Methoden in der Zell- und Molekularbiologie*. Stuttgart: Gustav Fischer-Verlag, 1984, pp 34–45

Reynolds EW: The use of lead citrate at high pH as an electron opaque stain in electron microscopy. *J Cell Biol* 17:208–212, 1963

Robards AW, Sleytr UB: *Low Temperature Methods in Biological Electron Microscopy*. Amsterdam: Elsevier, 1985

Schmidt A, Heid HW, *et al*: Desmosomes and cytoskeletal architecture in epithelial differentiation: cell type-specific plaque components and intermediate filament anchorage. *Eur J Cell Biol* 65:229–245, 1994

Schwartzendruber C, Burnett HI, Wertz PW, Madison KC, Squier CA: Osmium tetroxide and ruthenium tetroxide are complementary reagents for the preparation of epidermal samples for transmission electron microscopy. *J Invest Dermatol* 104:417–420, 1995

Schwarz H, Hohenberg H, Humbel BM. Freeze-substitution in virus research: a preview. In *Immuno-gold Electron Microscopy in Virus Diagnosis and Research*. Boca Raton: CRC Press, 1993, pp 349–375

Studer D, Michel M, Wohlwend M, Hunziker EB: Vitrification of articular cartilage by high-pressure freezing. *J Microsc* 179:321–332, 1995

Van den Bergh BIA, Schwartzendruber DC, Bos-Van der Geest A, *et al*: Development of an optimal protocol for the ultrastructural examination of skin by transmission electron microscopy. *J Microsc* 187(2):125–133, 1997

Van der Meulen J, Van den Bergh BIA, Mulder AA, Mommaas AM, Bouwstra JA, Koerten HK: The use of vibratome sections for the ruthenium tetroxide protocol: a key for optimal visualization of epidermal lipid bilayers of the entire human stratum corneum in transmission electron microscopy. *J Microsc* 184:67–70, 1996

Walther P, Eppenberger-Eberhardt M, Eppenberger HM, Müller M: Immunmarkierung an hochdruckgefrorenen adulten Herzmuskelzellen in Kultur. *Eur J Cell Biol* 61:98, 1993

Warner RR, Myers MC, Taylor DA: Electron probe analysis of human skin: Determination of the water concentration profile. *J Invest Dermatol* 90:218–224, 1988

Weibull CA, Christiansson A, Carlemalm E: Extraction of membrane lipids during fixation, dehydration and embedding of Acholeplasma laidlawi cells for electron microscopy. *J Microsc* 129(2):201–207, 1983

Weidenthaler B, Hausser I, Anton-Lamprecht I: Is filaggrin a filament-aggregating protein in vivo? *Arch Dermatol Res* 285:111–120, 1993

Wertz PW, Downing DT: Glycolipids in mammalian epidermis: structure and function in the water barrier. *Science* 217:2161–1262, 1982

Wertz PW, Downing DT: Ceramides of pig epidermis structure determination. *J Lipid Res* 24:759–765, 1983

Wijdeveled MMG, Koerten HK, Onderwater JJM, Parrott DP, Bouwstra JA: Visualization and electron diffraction on cryosections of stratum corneum: a utopia ? *J Microsc* 183(3):223–230, 1996

Wilson MT, Farmer MA, Karwoski CJ: Ultrastructure of frog retina after high-pressure freezing and freeze substitution. *J Microsc* 189(3):219–235, 1998